PHILOSOPHICAL MAGAZINE A, 2000, VOL. 80, NO. 8, 1955–1966

Texture investigation of hot-forged Nd–Fe–B magnets

S. RIVOIRARD†§, D. CHATEIGNER‡, P. DE RANGO†, D. FRUCHART†, R. PERRIER DE LA BATHIE† and J. L. SOUBEYROUX†

†Laboratoire de Cristallographie, CNRS, BP 166, 38042 Grenoble, France
‡Laboratoire de Physique de l'Etat Condense, Université du Maine, BP 535, 72085 Le Mans, France

[*Received 13 March 1999 and accepted in revised form 28 September 1999*]

ABSTRACT

This work represents one of the first attempts to probe the bulk crystallographic alignment of hot-forged Nd–Fe–B–Cu magnets using neutron diffraction techniques. Optimizing the microstructure induced by the hot-forging process is necessary to develop good magnetic properties. For that purpose, understanding the deformation mechanisms in terms of thermal and mechanical behaviour is of great importance. Ingots of Nd–Fe–B–Cu alloy were cast into steel tubes and hot forged at 980°C. The magnetic properties and induced texture of the magnet were investigated. The results show a fair correlation between microstructural parameters induced by the deformation mode and magnetic properties. Using neutron diffraction analysis, the pole figures revealed the existence of a texture that was more pronounced in the centre than in the periphery of the forged specimen. The good magnetic properties are the result of grain size reduction during forging combined with $Nd_2Fe_{14}B$ crystallite alignment (*c* axis aligned along the forging direction). As the Nd–Fe–B alloy is in a semisolid state at the processing temperature, the fraction of intergranular liquid phase has to be sufficient to allow alignment of the solid $Nd_2Fe_{14}B$ particles but not too important to allow internal stresses between solid grains (resulting in cracks and size reduction). The compromise optimizing the magnetic properties is studied in this work.

§1. INTRODUCTION

Nd–Fe–B-type magnets have been produced since 1984 based on the hard magnetic phase $Nd_2Fe_{14}B$ (Sagawa *et al.* 1984). In this type of material, $Nd_2Fe_{14}B$ grains are separated from each other by a non-magnetic Nd-rich intergranular phase. This microstructure, when optimized, is the key for inducing coercivity in the magnet. The size of the magnetic grains as well as the composition and repartition of the minor intergranular phase must be controlled to avoid the propagation of domain walls. Furthermore, texturing the intrinsically anisotropic magnetic grains leads to enhancement of the inductive force of the magnet, which can be doubled. Improvements in the processes used to develop optimized textures are needed for the engineering of high energy product $(BH)_{max}$ magnets. Processing by hot deformation of cast ingots is a potentially simple and economic route that currently attracts our attention (Nozières *et al.* 1994). Recently, much work has been done on developing slow strain-rate processes (such as upset forging of cast Pr–Fe-B–Cu

§Email: rivoirar@labs.polycnrs-gre.fr.

Philosophical Magazine A ISSN 0141–8610 print/ISSN 1460-6992 online
http://www.tandf.co.uk/journals

alloys (Mukai and Sakumoto 1989, Shimoda *et al.* 1989) or die upsetting of Nd–Fe–B powders (Lee *et al.* 1985)). However, slow strain rates do not induce any grain size reduction and previous processes such as hydrogen decrepitation desorption recombination (HDDR) (Takeshita and Nakayama 1989) or melt spinning (Croat *et al.* 1984) are needed to achieve coercivity before applying the hot deformation process (Liesert *et al.* 1998). On the contrary, high-strain-rate deformations should be efficient in grain-size reduction (by fragmentation) as well as in texturing the material. Such high strain rates are involved in hot rolling and have been investigated with $Nd_{17.5}Fe_{76}B_5Cu_{1.5}$ (Ferrante *et al.* 1994). We propose to go further in this study with the hot-forging process of Nd–Fe–B–Cu-type magnets. Cu is generally added to Nd–Fe–B alloys in order to enhance the hot workability, because this element lowers the melting point of the intergranular liquid phase (Nozawa *et al.* 1988).

Pure mechanical hot-deformation processes are efficient in enhancing magnetic anisotropy since the easy axis of magnetization (*c* axis) of the $Nd_2Fe_{14}B$ crystallites is perpendicular to the growing plane (largest dimensions of the crystallite). Alignment of the *c* axis is the most efficient when the crystallites are platelets. Platelets of solid magnetic particles ($Nd_2Fe_{14}B$ phase) can move and rotate easily within the liquid intergranular phase at the processing temperature. A crystallographic fibre texture results from the hot-forging process which leads to the alignment of the $Nd_2Fe_{14}B$ *c* easy axis of magnetization along the forging direction. Magnetic anisotropy is enhanced in most cases as a result of this texture development.

Here we report selected experiments planned to highlight the understanding of deformation mechanisms during the forging process. In particular it seems of first importance to find out the relationships between the magnetic properties and the mechanical parameters. Our analyses are based on both neutron texture studies and magnetic measurements.

§ 2. Experimental details

The Nd–Fe–B–Cu types of ingot (compositions $Nd_{11.8}Fe_{80.6}B_6Cu_{1.5}$, $Nd_{15.5}Fe_{78}B_5Cu_{1.5}$ and $Nd_{20}Fe_{73.5}B_5Cu_{1.5}$) used in this work were induction melted under an Ar atmosphere and cast in steel tubes. The as-cast ingot dimensions are 25 mm in height and 12 mm in diameter with a steel tube 1 mm thick. The ingots were then forged at 980°C under a strain rate of $10\,s^{-1}$. The steel tube was necessary to keep the magnetic material whole; otherwise it would have split into many small misoriented pieces.

The magnetic properties were measured at room temperature using a vibrating-sample magnetometer, up to 70 kOe ($5570\,kA\,m^{-1}$). The resultant hysteresis loops were adjusted for demagnetization with a geometric correction.

Neutron diffraction experiments were performed on beam line D1B at the Institut Laue–Langevin (ILL), Grenoble, using the Eulerian cradle geometry (figure 1). A monochromatic thermal neutron beam is provided from a neutron guide by a pyrolytic graphite (0002) monochromator which selects a wavelength $\lambda = 2.532$ Å. The diffracted intensity is collected in a position-sensitive multidetector with 400 cells covering 80° in a 2θ range (5 cells per degree). A routine procedure combining the capabilities of the ILL (Xrfit), CNRS (Illprep and Ill) and University of California, Berkeley (Wenk *et al.* 1998), packages enabled us to extract data and to obtain pole figures and orientation distributions as already described (Chateigner *et al.* 1997). The huge advantage of neutron diffraction lies in the lower absorption with respect to X-rays. This enables us to probe a much larger sample volume compared with

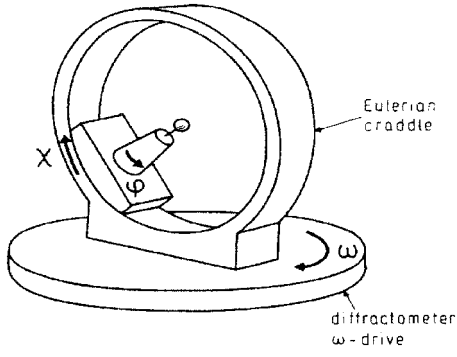

Figure 1. Eulerian cradle with definitions of the angles.

X-ray experiments, thus markedly increasing the statistics of counts owing to the large number of diffracting crystallites. Since the entire forged specimen can be tested, the experiment provides us with global information on the bulk with negligible surface effects.

A forged $Nd_{15.5}Fe_{78}B_5Cu_{1.5}$ specimen with height reduction of 82% and improved magnetic properties was studied by neutron diffraction. Two parts of the as-forged specimen were analysed: the centre and the edge. Each sample tested had a cubic shape with a 5 mm side. The degrees of crystallite alignment and comparisons between the central and the edge textures were established. The pole figures were extracted.

The pole figures were interpreted in terms of orientation distributions of a specific $[001]_c$ crystallite direction (the tetragonal axis of the $Nd_2Fe_{14}B$ phase) with respect to a reference sample frame based on the forging direction: $[001]_s$. The degree of texture is measured in multiples of random distribution (mrds). A perfect randomly oriented sample, for example a free powder, exhibits homogeneous pole figures with pole densities of 1 mrd in all directions.

Then χ scans were performed for two positions of the cradle ($\omega = 10^\circ$ and $\omega = 30^\circ$) in order to minimize as much as possible the blind area in the experimental pole figures. χ was varied from 0° to 90° in steps of 5° to provide the radial distribution of the pole densities. The pole figures were then symmetrized in order

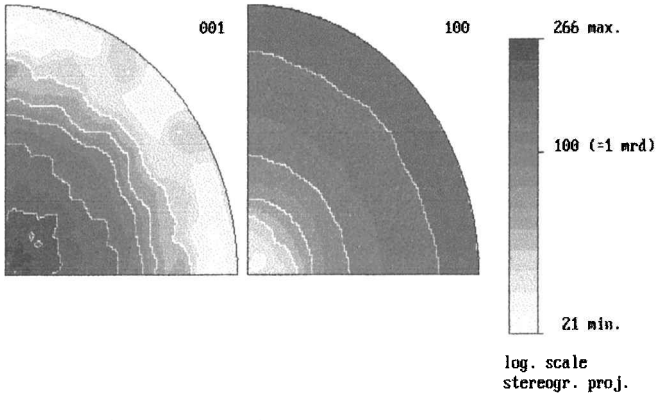

Figure 2. Scanning electron micrograph of the as-cast $Nd_{15.5}Fe_{78}B_5Cu_{1.5}$ alloy.

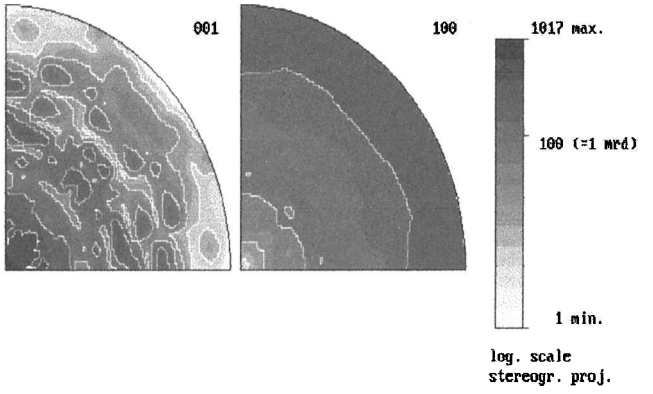

Figure 3. $[001]_s$ and $[100]_s$ inverse pole figures of the peripheral region of the as-forged sample.

to refine the orientation distribution (OD). In the case of a fibre texture the OD is fully described by the inverse figures (figures 2 and 3) calculated from the OD. These latter represent the distribution densities of all $\langle hkl \rangle_c$ directions along a specific direction of the sample, indexed with cubic pseudo-Miller indices $\langle HKL \rangle_s$.

§ 3. Results

The microstructure (figure 4) of the as-cast alloy consists of platelet-like $Nd_2Fe_{14}B$ grains (about 100 μm long and 10 μm thick) surrounded by the intergranular Nd-rich phase. Free Fe dendrites are visible too (about 15% in volume). As-cast samples do not show any permanent magnet properties mainly because of the presence of Fe (soft magnetic phase): $H_c = 0.2\,\text{kOe}$ ($15.9\,\text{kA m}^{-1}$), $B_r = 0.1\,\text{T}$, $BH_{max} = 0.03\,\text{MGOe}$ ($0.24\,\text{kJ m}^{-3}$).

Comparative magnetic measurements performed on the centre and the edge of the as-forged sample show better magnetic properties in the centre. Both remanence and coercivity are enhanced (figure 5).

A first φ scan ($\omega = 10^\circ$ and $\chi = 0^\circ$) confirmed the isotropic distribution of crystallographic orientations around the forging direction in both samples. This proves

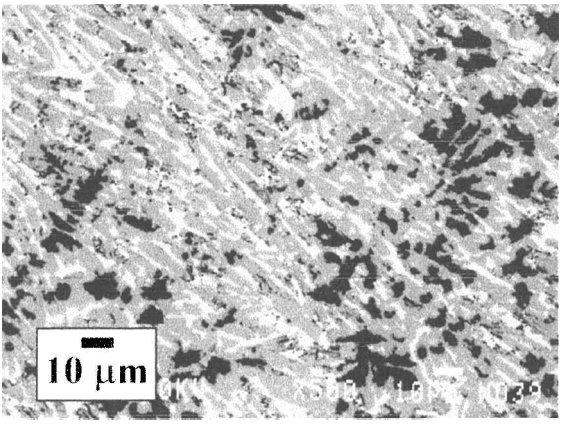

Figure 4. $[001]_s$ and $[100]_s$ inverse pole figure of the centre of the as-forged sample.

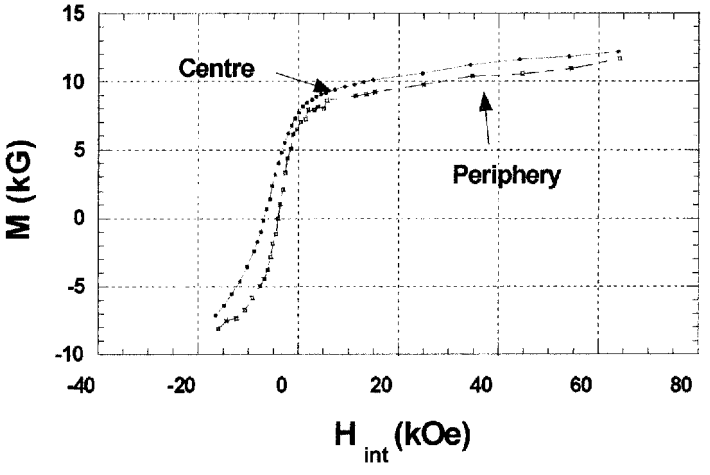

Figure 5. Demagnetization curve of the centre and the periphery of the forged specimen.

the fibre character of the texture. This texture is particularly suitable in terms of magnetic performances. With this configuration, remanence is enhanced in the forging direction, whereas it remains equal and reduced as much as possible along each of the directions belonging to the plane perpendicular to the forging direction $[001]_s$.

While the $\{001\}$ inverse pole figure shows which $\langle hkl \rangle_c$ crystallite axis is aligned along the forging direction, the $\{100\}$ inverse pole figure reveals axes lying in the plane perpendicular to the forging axis. Figures 2 and 3 clearly show that only $\langle 001 \rangle_c$ axes are aligned parallel to the forging direction, while all the perpendiculars to $\langle 001 \rangle_c$ are perpendicular to the forging direction. However, we note in $\{001\}$ inverse pole figures a weaker dispersion of the crystallites around the forging axis for the centre than for the edge of the specimen. This should be associated with a more pronounced texture at maximum of dispersion (corner of the inverse pole figure) in the centre (10.17 mrd) than at the periphery (2.66 mrd).

This result is in good agreement with the larger value of remanence obtained in the centre of the forged specimen where the alignment degree of crystallites is better and thus the contribution to magnetization markedly enhanced.

Fragmentation of the hard magnetic $Nd_2Fe_{14}B$ phase has already been observed in hot-rolled magnets (Ferrante *et al.* 1994). The same phenomenon is observed (figures 6 and 7) here with our forging process, leading to an important grain size reduction. This fragmentation occurs under external stress and is due to friction between the individual grains. This effect is the great advantage of this process because grain size reduction contributes to an increase in the coercivity. The second positive effect is the reaction that occurs in the cracks during forging between the free Fe and the Nd-rich intergranular phase. This reaction causes the disappearance of the soft magnetic Fe phase (figure 7).

As far as coercivity is concerned, magnetic measurements seem to correlate logically from the microstructure observed in scanning electron micrographs (figures 6 and 7). The $Nd_2Fe_{14}B$ grain size is larger in the periphery where the coercivity is lower. The grain size distribution centred on a few microns in the centre of the sample is shifted and centred around 10 μm at the periphery.

As can be seen in figures 3, 4, 6 and 7, forged samples are characterized by a heterogeneous microstructure related to the deformation mode. This is probably due

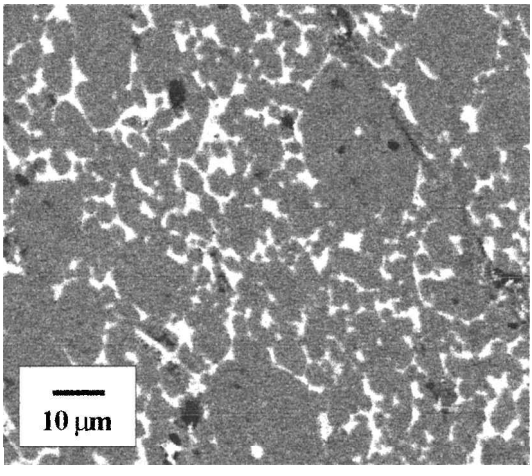

Figure 6. Scanning electron micrograph perpendicular to the forging direction of the periphery of the forged specimen (white, intergranular phase; black, free Fe; grey, $Nd_2Fe_{14}B$ grain).

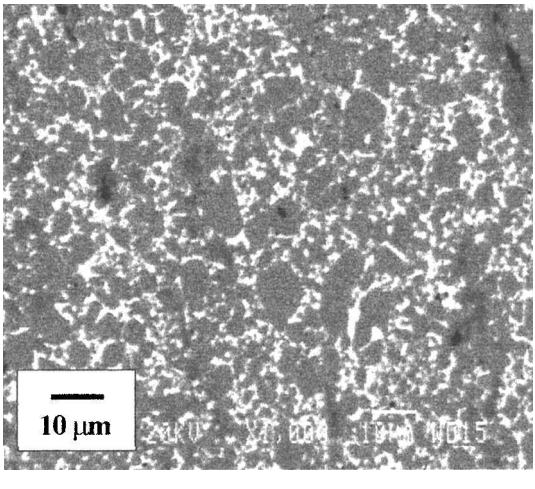

Figure 7. Scanning electron micrograph perpendicular to the forging direction of the centre of the forged specimen (white, intergranular phase; black, free Fe; grey, $Nd_2Fe_{14}B$ grain).

to the intergranular matter flow and the phase orientation during the deformation process. Inhomogeneous properties and microstructure should result from the inhomogeneous distribution of the liquid phase, which might be moved to the periphery of the sample on forging. Thus, a larger fraction of intergranular phase is expected at the periphery than in the centre of the specimen. An optical microscope pattern corroborates this effect very well (figure 8). At the interface between the magnetic material and the steel container, accumulation of the Nd-rich intergranular phase is revealed by a greater concentration of oxides (white contrast of neodymium oxide in figure 8) than on the rest of the surface of the cut sample.

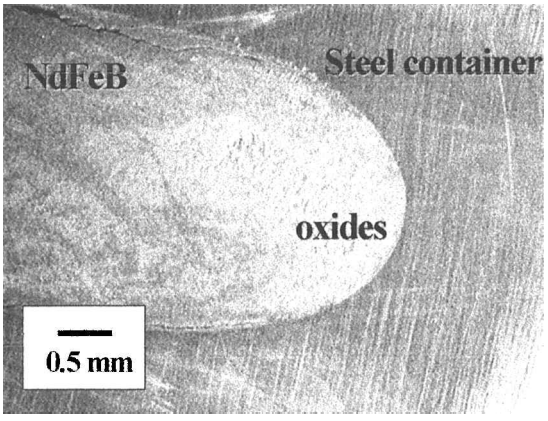

Figure 8. Optical micrograph parallel to the forging direction of the interface between the Nd–Fe–B material and the steel container (Nd oxides in white contrast).

In order to test the relevance of this 'liquid flow' phenomenon, two other samples with extreme compositions were forged: the first having a high Nd content ($Nd_{20}Fe_{73.5}B_5Cu_{1.5}$) and the second having a composition close to the stoichiometry of the $Nd_2Fe_{14}B$ phase ($Nd_{11.8}Fe_{80.6}B_6Cu_{1.5}$). The volume fraction of the intergranular liquid phase increases with increasing Nd content. The volume fraction of free Fe is estimated to be around 3% in the $Nd_{20}Fe_{73.5}B_5Cu_{1.5}$ as-cast alloy and 10% in the $Nd_{11.8}Fe_{80.6}B_6Cu_{1.5}$ composition. These samples were forged in the conditions described above and exhibited 91% and 76% height reduction respectively. During the forging process, the steel container exploded owing to the liquid flow strain in the first sample; thus the material was no longer constrained at the periphery. For this reason, we chose to study only the microstructure and magnetic properties of the centres of the two specimens.

Scanning electron micrographs of the forged samples (figures 9 and 10) reveal a finer and homogeneous microstructure in the $Nd_{11.8}Fe_{80.6}B_6Cu_{1.5}$ sample as well as a

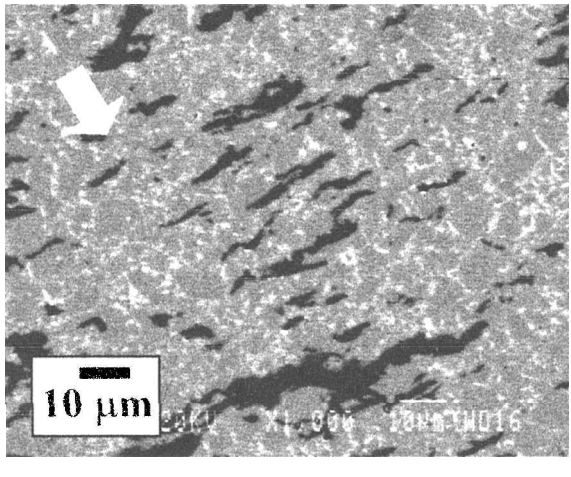

Figure 9. Scanning electron micrograph parallel to the forging direction of the $Nd_{11.8}Fe_{80.6}B_6Cu_{1.5}$ sample. The white arrow shows the forging direction.

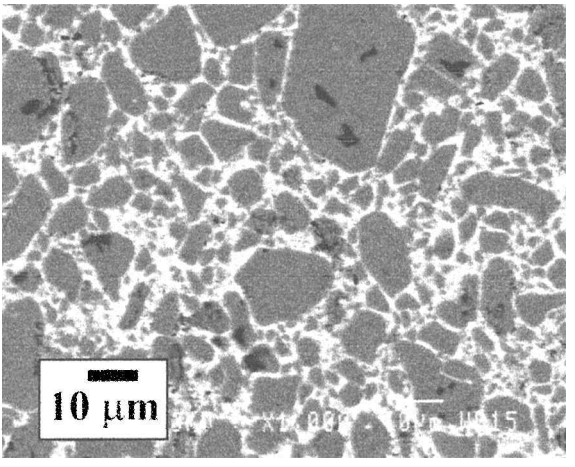

Figure 10. Scanning electron micrograph perpendicular to the forging direction of the $Nd_{20}Fe_{73.5}B_5Cu_{1.5}$ sample.

Table 1. Results of magnetic measurements for the three alloy compositions.

	$Nd_{11.8}Fe_{80.6}B_6Cu_{1.5}$	$Nd_{15.5}Fe_{78}B_5Cu_{1.5}$	$Nd_{20}Fe_{73.5}B_5Cu_{1.5}$
M_s (kG (T))	13.5 (1.35)	12 (1.2)	11.5 (1.15)
B_r (kG (T))	6 (0.6)	9 (0.9)	6 (0.6)
H_c (kOe (kA m^{-1}))	2.5 (199)	7 (557)	4.5 (358)
BH_{max} (MGOe (kJ m^{-3}))	2.5 (19.9)	10 (79.6)	3.6 (28.6)
$B_r^{\parallel}/B_r^{\perp}$	1.2	1.6	1.7

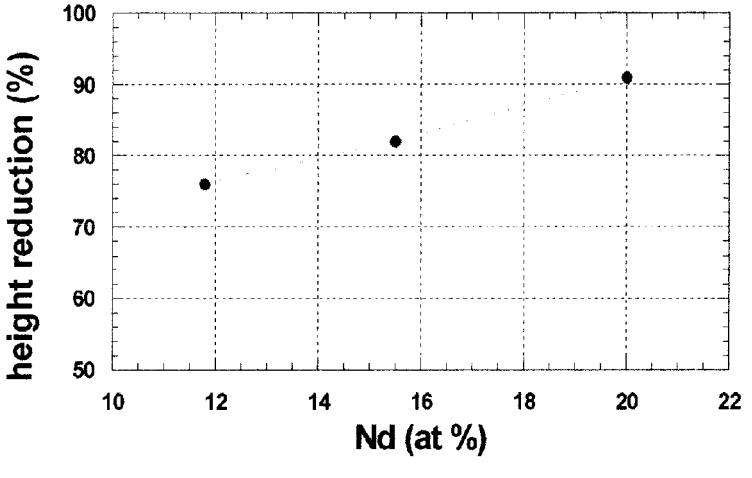

Figure 11. Height reduction as a function of Nd content for three samples under the same forging conditions.

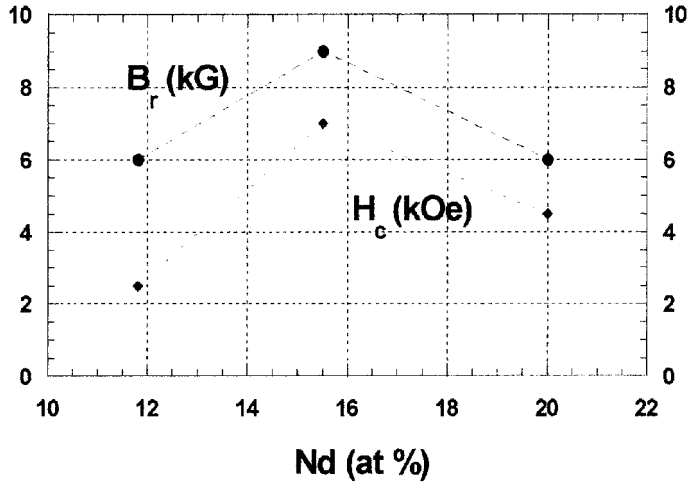

Figure 12. Remanence B_r and coercivity H_c as functions of Nd content for three samples under the same forging conditions.

large number of Fe dendrites. Under stress these dendrites expand perpendicular to the forging direction but are not brittle enough to be broken. The lack of Nd-rich intergranular phase creates additional difficulties; the free Fe dendrites do not react with the intergranular phase and do not dissolve during forging.

In the $Nd_{20}Fe_{73.5}B_5Cu_{1.5}$ sample the microstructure is heterogeneous; a large amount of grains were crushed but others remained coarse in their original platelet-like shape and with a size of many tens of microns. Few Fe dendrites are visible, in the largest grains only. The magnetic properties of each of the samples are listed in table 1. The anisotropy coefficient $B_r^{\parallel}/B_r^{\perp}$ is characteristic of the alignment of the $Nd_2Fe_{14}B$ crystallites.

The height reduction and the remanence and coercivity are shown as functions of Nd content in figures 11 and 12 respectively.

§4. Discussion

First we observe that, under the same forging conditions, the reduction height is enhanced with increasing Nd content (figure 11). It is well known that the degree of alignment of the crystallites and thus the magnetic properties of the sample strongly depend on the height reduction rate (Hatch *et al.* 1996). Increasing the Nd content reveals favourable crystallite alignment (see anisotropy coefficients in table 1). This can be easily understood if one considers the rearrangement process of platelets in a fluid. In principle, if the concentration of solid particles is low in the liquid, they will poorly interact (loss of contacts and frictions) and they will then align and rotate freely (Hatch *et al.* 1996). However, Ferrante *et al.* (1996) reported a more pronounced magnetic texture at the periphery of forged or pressed samples justified by the greater volume fraction of liquid in the periphery than in the centre, inducing better crystallite alignment. At first sight we would have to conclude similarly. In fact, neutron texture analyses reveal a more pronounced texture in the centre, where the volume fraction of intergranular liquid phase is known to be lower.

This should be attributed to different deformation states within the sample. Classical deformation maps obtained on materials forged with the same process

(Rambaud 1988) show an area of low deformation at the periphery of such forged samples whereas a cone of high deformation is designed in the centre and along diagonal lines. This could be an explanation for the less pronounced texture observed at the periphery of the specimen as revealed by neutron texture analysis.

The coercivity is expected to be lower at the periphery for the same reason. Moreover, in the liquid-rich region (and for the $Nd_{20}Fe_{73.5}B_5Cu_{1.5}$ sample), where the crystallite concentration is lower, fewer interactions between the grains will produce lower internal stresses. Moreover, the external forging stress will be less efficiently transmitted across the matter; thus the grain size reduction will not be so effective. This is revealed well by the scanning electron micrographs and by the data plotted in figure 5. The lower coercivity H_c value of the $Nd_{11.8}Fe_{80.6}B_6Cu_{1.5}$ sample has another origin. The grain size is fairly small $(10\,\mu m)$ but the coercivity is lowered by the high amount of free Fe remaining in the sample after forging. On the one hand, free Fe particles do not disappear (as for other samples under the combination of stress and high temperature conditions) because of the small amount of Nd-rich phase. On the other hand, where the Fe dendrites are locally too coarse, the size reduction of the $Nd_2Fe_{14}B$ grains is hindered by the plastic Fe dendrite which absorbs stresses for its own deformation. No cracks appear in the $Nd_2Fe_{14}B$ grains interacting with Fe dendrites. Fe dendrites act like softeners and locally the $Nd_2Fe_{14}B$ crystallites remain unchanged in terms of size and shape (figure 9).

Let us now compare the forging process with die upsetting. In the die upsetting, a powder is hot deformed at a very low strain rate $(10^{-3}\ s^{-1})$ (Croat *et al.* 1984). The diffusion precipitation mechanism is responsible for matter flow, under stress, from the misoriented crystallites to the benefit of the well oriented crystallites via the intergranular phase (Grünberger 1998). This mechanism leads to a more pronounced texture when the height reduction is increased (the applied stress and deformation rate being constant) but leads to poor orientation with increasing the Nd content (or decreasing applied stress). In the forging process, the driving force is not the applied stress by itself but rather the mechanical energy transmitted to the material (and consequently the deformation level achieved). For this reason, even when the plastic stress needed to the height reduction is decreased by increasing Nd content, an increased deformation level will be reached with the forging process and thus the texture will be enhanced. Moreover, die upsetting does not result in grain fragmentation. To obtain good die-upset products, the coercivity must exist in the sample before die upsetting.

However, diffusion processes during forging are not totally excluded. Differences between the composition of the intergranular phase before and after forging were noted by energy-dispersive spectroscopy analysis with the scanning electron microscope. In the as-cast state, the composition of the intergranular phase is near the Nd–Cu eutectic composition (only 3 at.% Fe is detected). In as-forged samples, the composition of the intergranular phase is different: Nd, 30 at.%, Fe, 60 at.%, Cu, 10 at.%. No abnormal $Nd_2Fe_{14}B$ grain growth was observed owing to the very fast deformation process but phase transformations do exist during forging. Until now, the driving parameters of these transformations have not been well identified. Forging is apparently not a pure mechanical process.

The results obtained for both the $Nd_{20}Fe_{73.5}B_5Cu_{1.5}$ and the $Nd_{11.8}Fe_{80.6}B_6Cu_{1.5}$ samples are of great interest to justify the different deformation modes as observed

on different parts of the same sample, but such an explanation follows the hypothesis that the liquid intergranular phase is moved to the periphery on forging. In fact, from scannning electron micrographs, a different amounts of intergranular phase between the centre and the periphery are not as evident. The difference in alignment between the centre and the periphery is not so marked. The matter flow is effective and it has to be taken into consideration as far as inhomogeneous modifications are concerned, but it is a subtle effect which is not a troubling parameter for using this forging process to produce anisotropic magnets. Thus, it has to be critically analysed and controlled prior to use of the forging process.

§ 5. Conclusion

Our results emphasize the aspect of microstructure for the development of forged magnets with good characteristics, not only in terms of coercivity but also in terms of grain alignment. On the one hand, the alignment seems to be better when the volume fraction of intergranular phase is increased because of better crystallite arrangements in the liquid phase at high temperatures. In this case, the grain size reduction is not efficient because the internal stresses between the grains are not sufficient. On the other hand, grain interaction via a minimum Nd-rich phase is necessary to allow the free Fe to dissolve in the bulk, leading to high coercivity (the soft magnetic phase Fe phase being the cause of low coercivity). We now aim to optimize the anisotropic macroscopic properties of the textured aggregate via selected processing conditions. This task is currently being pursued but the work presented in this paper provided a better quantitative understanding of the correlation between texture and physical characteristics.

Acknowledgement

Thanks are due to Rhodia for support of the general research programme of which this work forms a part.

References

Chateigner, D., Wenk, H. R., and Pernet, M., 1997, *J. appl. Crystallogr.,* **30**, 43.

Croat, J. J., Herbst, F., Lee, R. W., and Pinkerton, F. E., 1984, *J. appl. Phys.,* **55**, 2078.

Ferrante, M., Sinka, V., Assis, O. B. G., de Oliveira, I., and de Freitas, E., 1996, *Proceedings of the 14th Workshop on Rare Earth Magnets and their Applications,* edited by F. P. Missell, V. Villas-Boas, H. R. Rechenberg and F. J. C. Landgraf (Singapore: World Scientific), p. 255.

Ferrante, M., Sinka, V., Oliveira, I. L., and Assis, O. B. G., 1994, *Proceedings of the 13th International Workshop on Rare Earth Magnets and their Applications,* edited by I. R. Harris, pp. 655–661.

Grünberger, W., 1998, *Proceedings of the 15th Workshop on Rare Earth Magnets and their Applications,* edited by L. Schultz, p. 333.

Hatch, G. P., Williams, A. J., and Harris, I. R., 1996, *Proceedings of the 14th Workshop on Rare Earth Magnets and their Applications,* edited by F. P. Missell, V. Villas-Boas, H. R. Rechenberg and F. J. C. Landgraf (Singapore: World Scientific), p. 501.

Lee, R. W., Brewer, E. G., and Schaffel, N. A., 1985, *IEEE Trans. Magn.,* **21**, 1958.

Liesert, S., Kirchner, A., Grünberger, W., Handstein, A., De Rango, P., Fruchart, D., Schultz, L., and Müller, K. H., 1998, *J. Alloys Compounds,* **266**, 260.

Mukai, T., and Sakamoto, H., 1989, *Appl. Phys. Lett.,* **54**, 1597.

Nozawa, Y., Iwasaki, K., Taginawa, S., Togunaka, M., and Harada, H., 1988, *J. appl. Phys.,* **64**, 5285.

Nozières, J. P., Perrier de la Bâthie, R., and Lelièvre, M., 1994, US Pat. 5,356,489.

RAMBAUD, J. B., 1988, *Techniques de l'Ingénieur,* **M31**, M620.
SAGAWA, M., FUJIMORA, S., TOGAWA, N., YAMAMOTO, H., and MATSUURA, Y., 1984, *J. appl. Phys.,* **55**, 2083.
SHIMODA, T., AKIOKA, K., KOBAYASHI, O., YAMAGAMI, T., OHKI, T., MIYAGAWA, M., and YURI, T., 1989, *IEEE Trans. Magn.,* **25**, 4099.
TAKESHITA, T., and NAKAYAMA, R., 1989, *Proceedings of the Tenth International Workshop on Rare Earth Magnets and their Applications,* p. 551.
WENK, H. R., MATTHIES, S., DONOVAN, J., and CHATEIGNER, D., 1998, *J. appl. Crystallogr.,* **31**, 262.